DOI 10.1007/s10778-018-0901-3
International Applied Mechanics, Vol. 54, No. 4, July, 2018

FORCED VIBRATIONS OF PRE-STRESSED SANDWICH PLATE-STRIP WITH ELASTIC LAYERS AND PIEZOELECTRIC CORE*

A. Daşdemir

The dynamical stress field in a sandwich plate-strip is mathematically modeled using the piecewise-homogeneous body model and the three-dimensional linearized theory of electro-elastic waves in initially stressed bodies. The plate consists of a piezoelectric core perfectly bonded to elastic layers with initial stress, rests on a rigid foundation, and is subject to harmonic force. It is assumed that the piezoelectric material is poled perpendicularly to the free surface of the body. The governing system of partial differential equations of motion is solved by the finite-element method. The numerical results are presented, illustrating the effect of certain relationships of the problem of the propagation of stresses and electric displacements at the interfaces between the elastic layers and the piezoelectric core and between the plate-strip and the rigid foundation. The effect of the initial stress parameter and a change in the thickness of the piezoelectric core on the frequency response of the plate-strip is studied.

Keywords: piezoelectric core, finite-element method, harmonic force, sandwich plate-strip

1. Introduction. Sandwich structures are a kind of composite materials consisting of three layers, i.e., a core layer is bonded to two layers. The core material may be selected more flexible or harder than the others. The use of composite sandwich structures in many engineering applications such as building construction, aerospace, nuclear and civil infrastructure has been increasing especially due to their features such as good energy, sound absorption ability and high flexural stiffness. Hence, the subject has been intensively studied. The monograph [1] presents a detailed investigation on the subject.

Many researchers investigate many different problems based on various theories. Nayak et al. investigate the free vibration of composite sandwich plates by using a family of new Reddy type elements based on Reddy's higher-order theory [2]. Chakraborti and Seikh study the buckling of sandwich plates with laminated stiff layers subjected to partial edge compression based on a refined higher order shear deformation theory [3]. Hazard and Bouillard consider the passive damping of structural vibrations by the use of viscoelastic layers [4]. Pandit et al. develop an improved plate model to study the buckling of a laminated sandwich plate with transversely flexible core [5]. To analyze the static behavior of isotropic, sandwich, and laminated plates, Xiang et al. [6] present a new shear deformation theory. Li et al. [7] investigate the transient response of an orthotropic composite sandwich plate subjected to pointwise impulse loading with respect to a nonlinear high order core theory. Tu et al. [8] carve out a simple C^0 isoparametric finite-element formulation based on the refined higher-order shear deformation theory for the bending and free vibration of composite and sandwich laminate plates. Hasheminejad and Gheshlaghi [9] consider a three-dimensional elasticity-based formulation for the dynamic response of an arbitrarily thick simply supported FGM rectangular plate under

Department of Mathematics, Faculty of Arts and Sciences, Kastamonu University, Kastamonu, Turkey; e-mail: ahmetdasdemir37@gmail.com. Published in Prikladnaya Mekhanika, Vol. 54, No. 4, pp. 125–144, July–August, 2018. Original article submitted December 15, 2016.

* The author is a member of the research project supported by the Research Fund of Kastamonu University under project KÜ-BAP01/2015-3.

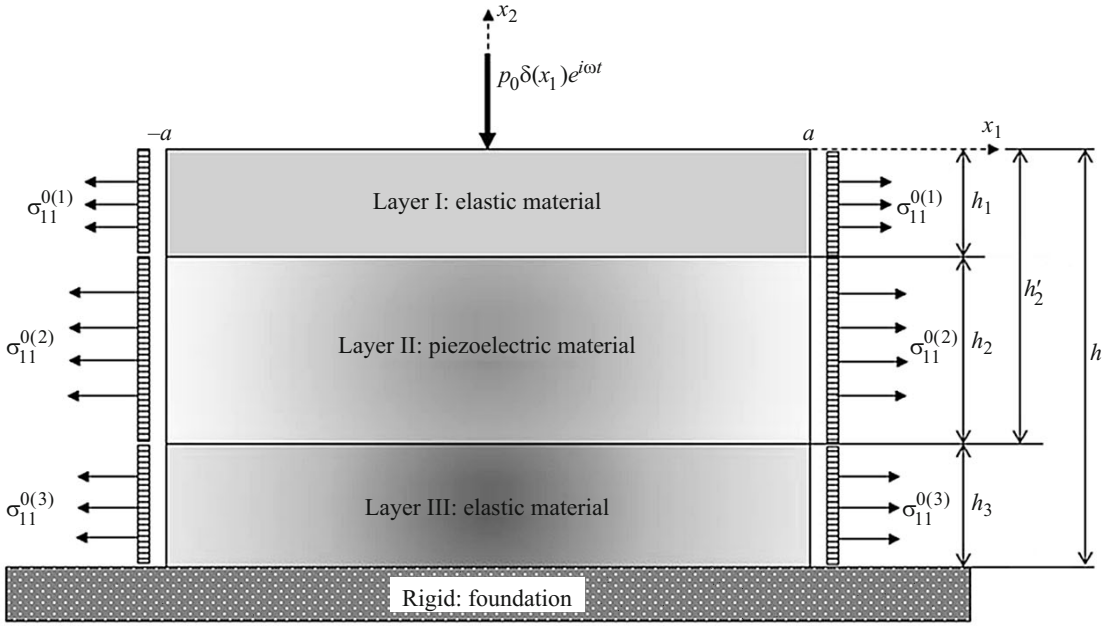

Fig. 1. Geometry of sandwich plate-strip with piezoelectric core.

transient loads of arbitrary spatial and temporal variations resting on a Winkler–Pasternak elastic foundation. Akbarov and Yahnioglu [10] study a buckling delamination problem for a sandwich plate-strip with piezoelectric face and elastic core layers that has two interface inner cracks by employing the finite-element method. Loja et al. [11] develop the static and dynamic behavior of functionally graded sandwich structures with piezoelectric skins by B-spline finite strip models. Shahraeeni et al. [12] analyze analytically free and forced vibration of piezoelectric laminated plates coupled with rectangular acoustic cavities based on Kirchhoff plate model. Sanker et al. [13] present the dynamic instability behavior of sandwich panels with carbon nanotube (CNT) reinforced facesheets under a periodic load.

To the author's knowledge, the forced vibration of a pre-stressed sandwich plate-strip with a piezoelectric core perfectly bonded to two elastic layers subjected to a harmonic force resting on a rigid foundation has not been studied so far. To address the issue, the mathematical modeling of the problem under consideration is analytically solved by employing the finite-element method. Most significant contributions of this work include the investigation of the effect of the different problem dependences on the frequency response of the sandwich plate-strip.

2. Statement of Problem. Consider a sandwich plate-strip with length $2a$ and thickness h under the action of a time-harmonic force resting on a rigid foundation, as depicted in Fig. 1. It consists of a piezoelectric core with thickness h_2 perfectly bonded to two isotropic layers with thicknesses h_1 and h_3, respectively. The poling direction of the piezoelectric material is assumed along the Ox_2-axis.

The locations of the layers are determined by the Lagrangian coordinates, which coincide with Cartesian coordinates in the natural state. The quantities referred to the upper, core, and lower layers of the plate-strip are denoted by the superscripts "(1)", "(2)", and "(3)", respectively, and the additional superscript 0 refers to the initial state. It is assumed that the length of the plate-strip along the Ox_3-axis is infinite. However, since the force applied to the body extends to infinity along the Ox_3-axis, the plane strain state appears on the Ox_1x_2 plane. All investigations are therefore made in the Ox_1x_2 plane. The plate-strip occupies the domain $B = B_1 \cup B_2 \cup B_3$, where

$$B_1 = \{(x_1, x_2): -a \le x_1 \le a,\ -h_1 \le x_2 \le 0\}, \tag{1}$$

$$B_2 = \{(x_1, x_2): -a \le x_1 \le a,\ -h_2' \le x_2 \le -h_1\}, \tag{2}$$

$$B_3 = \{(x_1, x_2): -a \le x_1 \le a,\ -h \le x_2 \le -h_2'\}. \tag{3}$$

The general forms of the differential equations of motion for the small initial deformation can be expressed as follows [14, 15]:

$$\sigma_{ij,j}^{(m)} + (\sigma_{kj}^{0,(m)} u_{i,k}^{(m)})_{,j} = \rho^{(m)} \ddot{u}_i^{(m)}, \tag{4}$$

$$D_{i,i}^{(m)} + (D_j^{0,(m)} u_{i,j}^{m})_{,i} = 0, \tag{5}$$

where $i, j, k = 1, 2$, $m = 1, 2, 3$, $\rho^{(m)}$ is the corresponding mass density in the natural state, $u_i^{(m)}$ and $D_i^{(m)}$ denote the mechanical and electrical displacements with respect to corresponding coordinate x_i, $\sigma_{ij}^{(m)}$ is the stress tensor, $\sigma_{kj}^{0,(m)}$ is the initial stress tensor, and $D_j^{0,(m)}$ is the initial electrical displacement. The overdot denotes time differentiation and the comma followed by the subscript "*i*" indicates space-coordinate differentiation. Here and below, the repeated index in the subscript denotes summation over that index. It should be noted that Eq. (4) is written for both the elastic phase and the piezoelectric phase. But Eq. (5) vanishes for the elastic phase since it concerns the electrical displacements.

Before compounding layers to each other and to the rigid foundation, they are stretched or compressed separately in the Ox_1 direction by uniformly distributed normal forces. Hence, uniaxial homogenous initial stress state occurs in the plate-strip. This initial stress is determined by utilizing the linear theory of the electro-elasticity as

$$\sigma_{11}^{0,(m)} = q^{(m)}, \quad \sigma_{ij}^{0,(m)} = 0 \quad \text{for all} \quad ij \neq 11, \tag{6}$$

where $q^{(m)}$ is a known constant for each layer. According to all the foregoing assumptions and due to the character of the piezoelectric material, an axial homogenous initial electric displacement emerges in the piezoelectric layer as

$$D_1^{0,(2)} = D_1^0 \quad \text{and} \quad D_2^{0,(2)} = D_2^0 = 0. \tag{7}$$

Note that the initial stress and initial electric displacement cannot be independent of each other. They must be self-consistent. This statement will be explained later.

The mechanical and geometrical relations for the isotropic elastic material and the piezoelectric material can respectively be written as

$$\sigma_{ij}^{(l)} = \lambda^{(l)} \varepsilon_{\theta\theta}^{(l)} \delta_{ij} + 2\mu^{(l)} \varepsilon_{ij}^{(l)}, \tag{8}$$

$$\sigma_{ij} = c_{ijkl} \varepsilon_{kl} - e_{kij} \varphi_{,k}, \quad D_i = e_{ikl} \varepsilon_{kl} - \gamma_{ik} \varphi_{,k}, \tag{9}$$

where $l = 1, 3$, $\lambda^{(m)}$, and $\mu^{(m)}$ are the Lamé constants for the elastic phase, c_{ijkl}, e_{kij}, and γ_{ik} are the mechanic, piezoelectric, and dielectric constants, respectively, for the piezoelectric phase, δ_{ij} is the Kronecker delta, φ is the electric potential, $\varepsilon_{ij}^{(m)} = \frac{1}{2}(u_{i,j}^{(m)} + u_{j,i}^{(m)})$ is the strain tensor. Note that, since the piezoelectric material is only in the intermediate layer, the superscript is omitted.

Now the boundary and contact conditions are considered.

According to the foregoing discussions, the boundary conditions on the free surface and on the ends of the plate-strip are described as

$$\sigma_{12}^{(1)}\Big|_{x_2=0} = 0, \quad \sigma_{22}^{(1)}\Big|_{x_2=0} = -p_o \delta(x_1) e^{i\omega t}, \tag{10}$$

$$(q^{(m)} u_{j,1}^{(m)} + \sigma_{1j}^{(m)})\Big|_{x_1 = \mp a} = 0, \tag{11}$$

$$\left(D_1 + D_1^0 u_{1,1}\right)\Big|_{\substack{x_1 = \mp a \\ -h_2' < x_2 < -h_1}} = 0. \tag{12}$$

The surfaces of the piezoelectric layer are assumed to be mechanically free and electrically open. The boundary conditions can therefore be written as

$$\varphi\big|_{\substack{x_1=\mp a\\ -h_2'<x_2<-h_1}}=0 \quad \text{and} \quad \varphi\big|_{\substack{x_2=-h_1,-h_2'\\ -a<x_1<-a}}=0. \tag{13}$$

It is assumed that, at the interfaces between the layers and between the plate-strip and the rigid foundation, there exists a completely clamping state. In this case, the complete clamped conditions are

$$\sigma_{i2}^{(1)}\Big|_{x_2=-h_1}=\sigma_{i2}^{(2)}\Big|_{x_2=-h_1}, \quad \sigma_{i2}^{(2)}\Big|_{x_2=-h_2}=\sigma_{i2}^{(3)}\Big|_{x_2=-h_2}, \tag{14}$$

$$u_i^{(1)}\Big|_{x_2=-h_1}=u_i^{(2)}\Big|_{x_2=-h_1}, \quad u_i^{(2)}\Big|_{x_2=-h_2}=u_i^{(3)}\Big|_{x_2=-h_2}, \tag{15}$$

$$u_j^{(3)}\Big|_{x_2=-h}=0. \tag{16}$$

This completes the formulation of the problem and the investigation of the governing field equations.

3. FEM Modeling. An analytical solution of the considered problem cannot be obtained; therefore, to solve this problem, the finite-element method (FEM) is employed. Before starting solution, certain preparations are made. First of all, a dimensionless coordinate system is introduced as

$$\hat{x}_1=\frac{x_1}{h}, \quad \hat{x}_2=\frac{x_2}{h}. \tag{17}$$

In addition, recall the lineal load applied to the plate-strip is assumed to be time-harmonic, with frequency ω, as $p_o\delta(x_1)e^{i\omega t}$. Thus, all the dependent variables can be written in the form

$$\{\sigma_{ij},u_i,\varepsilon_{ij},D_i\}^{(m)}(x_1,x_2,t)=\{\overline{\sigma}_{ij},\overline{u}_i,\overline{\varepsilon}_{ij},\overline{D}_i\}^{(m)}(x_1,x_2)e^{i\omega t}, \tag{18}$$

where the overbar represents the amplitude of the corresponding quantities. After the coordinate transformation in (17) and substituting expression (18) into the foregoing equations and conditions, the same equations and boundary-contact conditions are obtained for the amplitude of the sought quantities by replacing the terms $\partial^2 u_j^{(m)}/\partial t^2$ and $p_o\delta(x_1)e^{i\omega t}$ with $-\omega^2 u_j^{(m)}$ and $p_o\delta(x_1)$, respectively.

To obtain FEM modeling of the last boundary-contact problem, the following functional is presented:

$$J(u^{(m)})=\frac{1}{2}\sum_{m=1}^{3}\int_B\Big[T_{ij}^{(m)}u_{j,i}^{(m)}+\rho^{(m)}\omega^2h^2\{(u_1^{(m)})^2+(u_2^{(m)})^2\}\Big]dB$$

$$+\frac{1}{2}\int_{B_2}S_i\varphi_{,i}dB_2+\int_{-a/h}^{a/h}\frac{p_o\delta(x_1)}{\mu^{(1)}}u_2^{(1)}\Big|_{x_2=0}dx_1, \tag{19}$$

where

$$T_{ij}^{(m)}=\sigma_{ij}^{(m)}+\sigma_{in}^{0,(m)}u_{j,n}=w_{ijkn}u_{n,k}^{(m)}+t_{ijk}\varphi_{,k},$$

$$S_i=D_i+D_n^0u_{i,n}=t_{kni}u_{n,k}+r_{ik}\varphi_{,k}. \tag{20}$$

According to the constitutive equation (9), the notation in (20) can clearly be written for the piezoelectric phase as

$$w_{1111}=c_{11}+q, \quad w_{1122}=c_{13}, \quad w_{1212}=c_{44}, \quad w_{1221}=c_{44}+q,$$

$$w_{2112}=c_{44}, \quad w_{2121}=c_{44}, \quad w_{2211}=c_{13}, \quad w_{2222}=c_{33},$$

$$t_{111}=D_1^0, \quad t_{121}=e_{15}, \quad t_{211}=e_{15}, \quad t_{122}=D_1^0,$$

$$t_{222} = e_{33}, \quad t_{112} = e_{31}, \quad r_{11} = -\gamma_{11}, \quad r_{22} = -\gamma_{33}. \tag{21}$$

It is should be considered that, while $T_{ij}^{(m)}$ is computed, t_{1ii} is equal to zero. Note that the notation in (21) coincides with that for the elastic layers and $c_{11} = c_{33} = \lambda^{(l)} + 2\mu^{(l)}$, $c_{13} = \lambda^{(l)}$, $c_{44} = \mu^{(l)}$, $q = q^{(l)}$, $e_{31} = e_{15} = e_{33} = 0$, and $\gamma_{11} = \gamma_{33} = 0$. In addition, all the components that are not inserted into relations (21) are equal to zero. It is easy to confirm that

$$w_{ijkn} = w_{nkji}, \quad t_{111} = t_{122}, \quad \text{and} \quad t_{ijk} = t_{jik}. \tag{22}$$

To show the validity of the functional presented in (19), Gauss's theorem is used. Taking the symmetry conditions in (22) into account,

$$\delta J(u^{(m)}) = \delta\left(\frac{1}{2} \sum_{m=1}^{3} \int_B \left[w_{ijkn}^{(m)} u_{n,k}^{(m)} u_{j,i}^{(m)} + t_{ijk} u_{j,i}^{(m)} \varphi_{,k} + \rho^{(m)} \omega^2 h^2 \left(u_1^{(m)} + u_2^{(m)} \right)^2 \right] dB \right.$$

$$\left. + \frac{1}{2} \int_{B_2} [t_{kni} u_{n,k} \varphi_{,i} + r_{ik} \varphi_{,k} \varphi_{,i}] dB_2 + \int_{-a/h}^{a/h} \frac{p_o \delta(x_1)}{\mu^{(1)}} u_2^{(1)} \Big|_{x_2=0} dx_1 \right)$$

$$= \frac{1}{2} \sum_{m=1}^{3} \int_B \left[(w_{ijnk}^{(m)} + w_{knji}^{(m)}) u_{n,k}^{(m)} \delta u_{j,i}^{(m)} + (t_{ijk} + t_{jik}) \delta u_{j,i} \varphi_{,k} + 2\rho^{(m)} \omega^2 h^2 u_j^{(m)} \delta u_j^{(m)} \right] dB$$

$$+ \int_{B_2} [t_{kni} u_{n,k} \delta\varphi_{,i} + r_{ik} \varphi_{,i} \delta\varphi_{,k}] dB_2 + \int_{-a/h}^{a/h} \frac{p_o \delta(x_1)}{\mu^{(1)}} \delta u_2^{(1)} \Big|_{x_2=0} dx_1$$

$$= \sum_{m=1}^{3} \int_B [w_{ijnk}^{(m)} u_{n,k}^{(m)} \delta u_{j,i}^{(m)} + t_{ijk} \delta u_{j,i} \varphi_k + \rho^{(m)} \omega^2 h^2 u_j^{(m)} \delta u_j^{(m)}] dB$$

$$+ \int_{B_2} [t_{kni} u_{n,k} \delta\varphi_i + r_{ik} \varphi_{,i} \delta\varphi_{,k}] dB_2 + \int_{-a/h}^{a/h} \frac{p_o \delta(x_1)}{\mu^{(1)}} \delta u_2^{(1)} \Big|_{x_2=0} dx_1$$

$$= \sum_{m=1}^{3} \int_S [w_{ijnk}^{(m)} u_{n,k}^{(m)} + t_{ijk} \varphi_{,k}] n_i \delta u_j dS + \int_{-a/h}^{a/h} \frac{p_o \delta(x_1)}{\mu^{(1)}} \delta u_2^{(1)} \Big|_{x_2=0} dx_1$$

$$- \sum_{m=1}^{3} \int_B \left[(w_{ijnk}^{(m)} u_{n,k}^{(m)})_{,i} + (t_{ijk} \varphi_{,k})_{,i} - \rho^{(m)} \omega^2 h^2 u_j^{(m)} \right] \delta u_j^{(m)} dB$$

$$+ \int_{B_2} [t_{kni} u_{n,k} + r_{ik} \varphi_{,i}] n_i \delta\varphi dS_2 - \int_{B_2} \left[(t_{kni} u_{n,k})_{,i} + (r_{ik} \varphi_i)_{,k} \right] \delta\varphi dB_2, \tag{23}$$

in which S_2 denotes the boundary of the domain B_2 and n_i is the components of $\boldsymbol{n}$, the outward unit vector normal to all the boundaries in the domain B.

Considering the statement

$$\delta J(\boldsymbol{u}^{(m)}) = 0, \tag{24}$$

the equations of motion and the corresponding boundary-contact conditions given in (4)–(5) and (10)–(16) are obtained. Thus, the validity of functional (19) suggested for the mathematical modeling is proved.

TABLE 1. Values of material characteristics

Property	Elastic layer		Core Layer
	Aluminum	Steel	$BaTiO_3$
E, GPa	70	210	—
ν	0.35	0.29	—
c_{11}, GPa	—	—	150
c_{13}, GPa	—	—	66
c_{33}, GPa	—	—	146
c_{44}, GPa	—	—	44
e_{31}, cm^{-2}	—	—	–4.35
e_{33}, cm^{-2}	—	—	17.5
e_{15}, cm^{-2}	—	—	11.4
γ_{11}, nFm^{-1}	—	—	11.15
γ_{33}, nFm^{-1}	—	—	12.6
ρ, kgm^{-3}	2712	7850	7280

For the functional given in (19), the FEM modeling of the problem is created by the virtual work principle and the standard Rayleigh–Ritz method [17]. According to this approach, the domain B is divided into a finite element of sub-domains whose structures are four-node smooth rectangular elements. It is immediately specified that the number of finite elements is determined from the desired numerical convergence requirement. According to the well-known procedure, after fairly extensive mathematical arrangements, a system of algebraic equations is obtained as

$$(\boldsymbol{K} - \omega^2 \mathrm{M})\widetilde{\boldsymbol{u}} = \boldsymbol{F}, \tag{25}$$

where $\boldsymbol{K}$ is the stiffness matrix, M is the mass matrix, $\widetilde{\boldsymbol{u}}$ is the column vector of unknown nodal displacements, and $\boldsymbol{F}$ is the force vector. To reduce the size of the present paper the explicit forms of the above-stated matrices and vectors are omitted. However, their explicit forms are directly derived from Eqs. (19) and (23) by using the procedure considered. This completes the FEM modeling of the problem.

4. Numerical Results. Getting started with this section, certain remarks are made to more easily understand the numerical investigations. Some notation is first introduced as

$$e = \frac{E^{(3)}}{E^{(1)}}, \qquad \Omega^{(l)} = \omega h \sqrt{\frac{\rho^{(l)}}{\mu^{(l)}}}, \quad \text{and} \quad \eta^{(l)} = \frac{q^{(l)}}{\mu^{(l)}} \tag{26}$$

for the elastic layers and

$$\Omega = \omega h \sqrt{\frac{\rho}{c_{44}}} \quad \text{and} \quad \eta = \frac{q}{c_{44}} \tag{27}$$

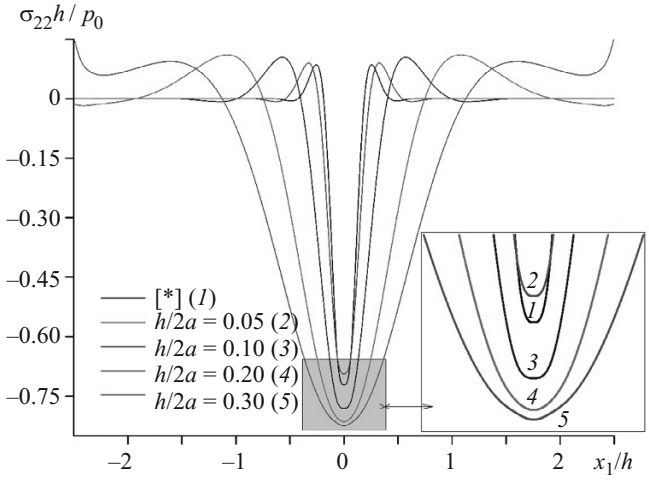

Fig. 2. Variation of $\sigma_{22}h/p_0$ with x_1/h for different thickness ratios under Case II on the bottom surface.

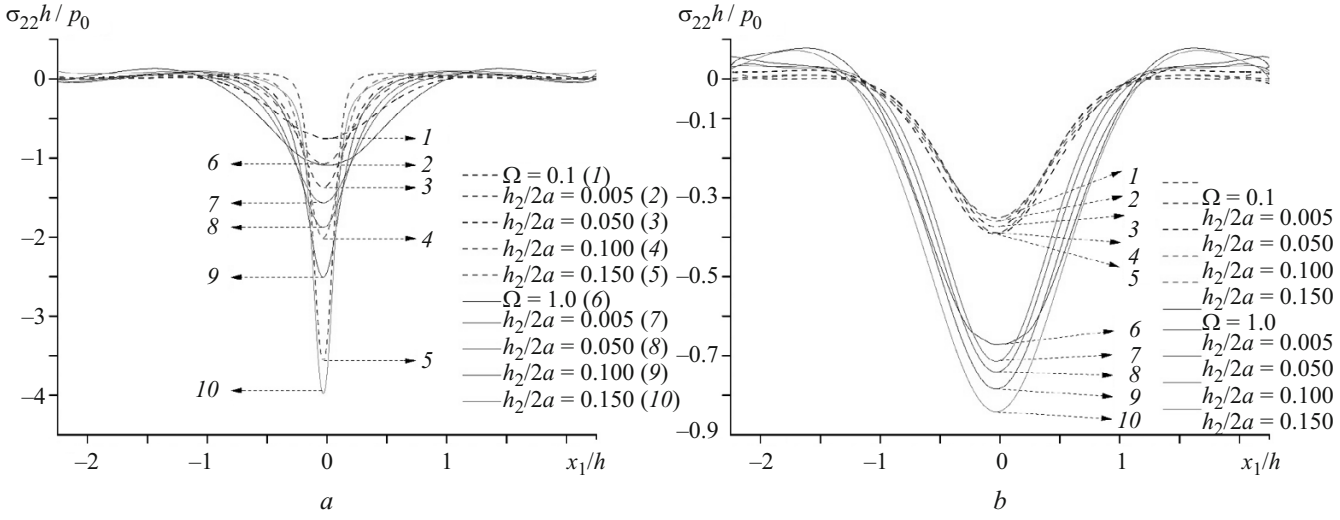

Fig. 3. Variations of $\sigma_{22}h/p_0$ with x_1/h for different piezoelectric thickness ratios under Case I at the upper (*a*) and bottom (*b*) interfaces.

for the piezoelectric core. In (26) and (27), $E^{(1)}$ is Young's modulus for the elastic layer, $\Omega^{(m)}$ is the dimensionless frequency parameter, and $\eta^{(m)}$ is the initial stress parameter.

Throughout the paper, all the numerical investigations are made at the interfaces between the upper elastic layer and the piezoelectric core (named "upper interface"), between the piezoelectric core and the lower elastic layer (named "lower interface"), and between the plate-strip and the rigid foundation (named "bottom surface"). Note that, when the corresponding parameters are equal, the superscript "(*m*)" will be omitted. It is assumed that, for all the examples considered, the two elastic layers have the same thickness ($h_1 = h_3$), and the material $BaTiO_3$ is selected for the piezoelectric core. The following cases are also considered for $h/2a = 0.2$, $h_2/h = 0.5$, $\Omega = 0$, and $\eta = 0$ unless specified otherwise:

Case I: Aluminum (Upper layer) + $BaTiO_3$ (Core layer) + Steel (Lower layer)

Case II: $$E^{(1)} = E^{(3)} = 1, \quad \nu^{(1)} = \nu^{(3)} = 0.33.$$

The electromechanical properties of the materials considered are listed in Table 1. Changing values in any case will be specifically indicated.

As previously mentioned, the self-consistent condition of the initial stress (stretching or compressing) field for the piezoelectric phase should be satisfied. In this study, only a uniformly distributed normal initial stress field is considered. Then

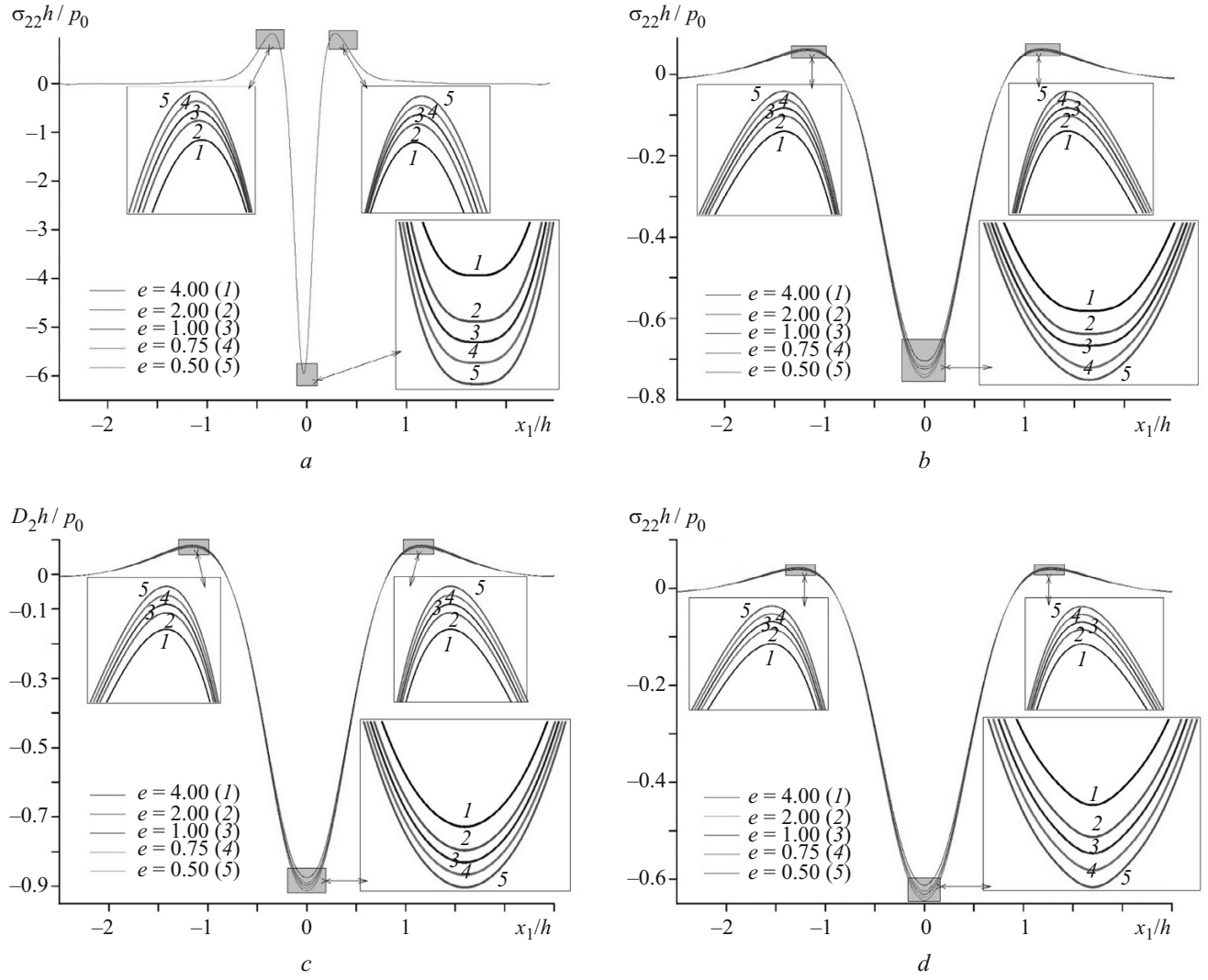

Fig. 4. Variations of $\sigma_{22}h/p_0$ and D_2h/p_0 with x_1/h for different values of e under Case II and $\Omega = 0.3$ at the upper (*a*), lower (*b*, *c*), and bottom (*d*) interfaces.

considering the constitutive equations, the equation $D_1^0 = q^{(2)}(c_{13}e_{33} - c_{33}e_{31})/(c_{13}^2 - c_{11}c_{33})$ can directly be derived for the piezoelectric phase. The values of the initial stress parameter $\eta^{(m)}$ are chosen at asymmetric interval –0.07 to 0.07.

Before starting to present numerical results, the validity of the numerical algorithms and programs composed by the author must be verified. To do this, certain special cases are considered, and it will be shown that the obtained numerical results converge to the previous ones and the findings agree well with the foregoing discussion.

In Fig. 2, the distribution of the normal stress $\sigma_{22}h/p_0$ with respect to the line x_1/h on the bottom surface for Case II and $h_2 << h$ is displayed. This figure gives the opportunity to compare the numerical results obtained by using the present FEM algorithm with the ones given by Uflyand [18] for a plate with infinite length. Note that the starred graph in Fig. 2 means the one in [18]. The geometry of the body begins to resemble a semi-infinite structure as $h/2a \to 0$. In this case, the present numerical results must converge to the corresponding ones obtained in [18] as $h/2a \to 0$. This statement is demonstrated by the graphs in Fig. 2 plotted on the bottom surface.

Figure 3 shows the distribution of the normal stress $\sigma_{22}h/p_0$ with respect to the line x_1/h for different thicknesses of the piezoelectric core under Case I at the upper interface and on the bottom surface. Note that the notation [$\Omega = \bullet$] means the corresponding one in [16], and the solid (dashed) lines are plotted for $\Omega = 0.1$ ($\Omega = 1.0$). The geometry of the plate-strip begins to resemble that in [16] as $h_2 \to 0$. It can easily be observed from the graphs in Fig. 3 that the numerical results converge to the corresponding ones given in [16] for both interface and bottom surface as $h_2 \to 0$.

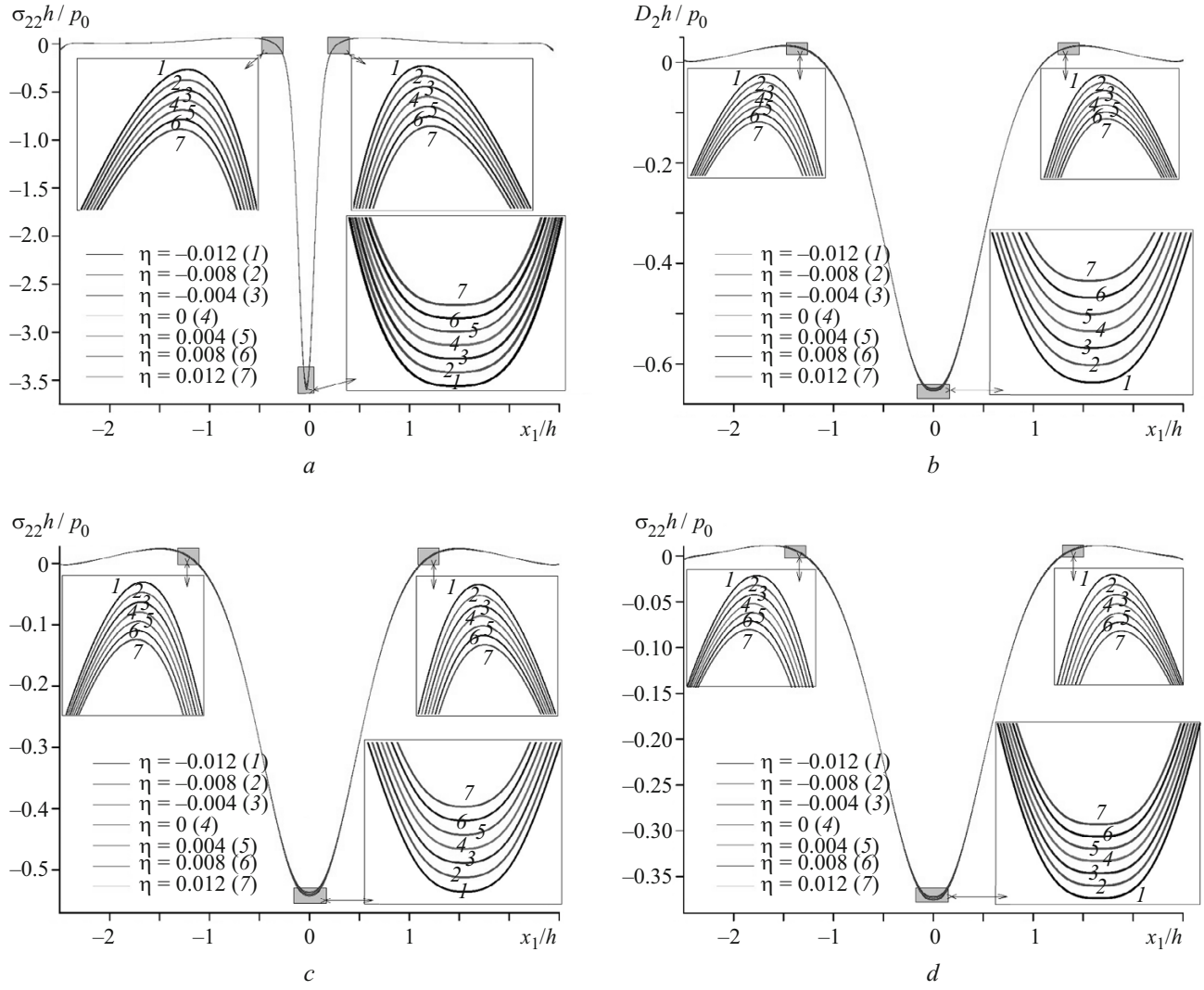

Fig. 5. Variations of $\sigma_{22}h/p_0$ and D_2h/p_0 with x_1/h for different values of η under Case I and $\Omega = 0.3$ at the upper (*a*), lower (*b*, *c*), and bottom (*d*) interfaces.

Now, the effect of the ratio of Young's modulus of the elastic layers on $\sigma_{22}h/p_0$ and D_2h/p_0 along the line x_1/h is given in Fig. 4 under Case II, $h_2/h = 0.75$ and $\Omega = 0.3$. According to the well-known mechanical consideration, an increase in the ratio *e* must give rise to a decrease in the absolute values of $\sigma_{22}h/p_0$ for a multi-layered body. Indeed, this prediction is clearly observed from the graphs in Fig. 4. In addition, it can be said that there exist certain locations where the values of $\sigma_{22}h/p_0$ and D_2h/p_0 are independent of the ratio *e*.

The numerical results obtained from Figs. 2 and 3 show that, in certain special cases, the distributions of the stress $\sigma_{22}h/p_0$ converge to the previous ones. Moreover, the findings in Fig. 4 agree well with the well-known foregoing mechanical considerations. In this way, the validity and trustiness of the algorithm and programs have been shown.

In Fig. 5, the effect of the initial stretching (compressing) η on the distribution of $\sigma_{22}h/p_0$ and D_2h/p_0 with respect to the line x_1/h under Case I, $h_2/h = 0.75$ and $\Omega = 0.3$ at the upper and lower interfaces and on the bottom surface is displayed. It can be shown from the graphs in Fig. 5 that, under $-x_1^*/h < x_1/h < x_1^*/h$ the absolute values of $\sigma_{22}h/p_0$ and D_2h/p_0 decrease (increase) with increasing initial stretching (compressing) parameter. But under $-x_1^{**}/h < x_1/h < -x_1^*/h$ and $x_1^*/h < x_1/h < x_1^{**}/h$, the absolute values of $\sigma_{22}h/p_0$ and D_2h/p_0 decrease with (increasing) initial stretching (compressing) parameter. Note that the values of x_1^*/h and x_1^{**}/h can be observed in Fig. 5 and are different at the upper and lower interfaces and on the bottom surface. As can be seen from Fig. 5, the effect of the initial stretching parameter applied to the body on $\sigma_{22}h/p_0$ and D_2h/p_0 is the opposite of that for the initial compressing parameter.

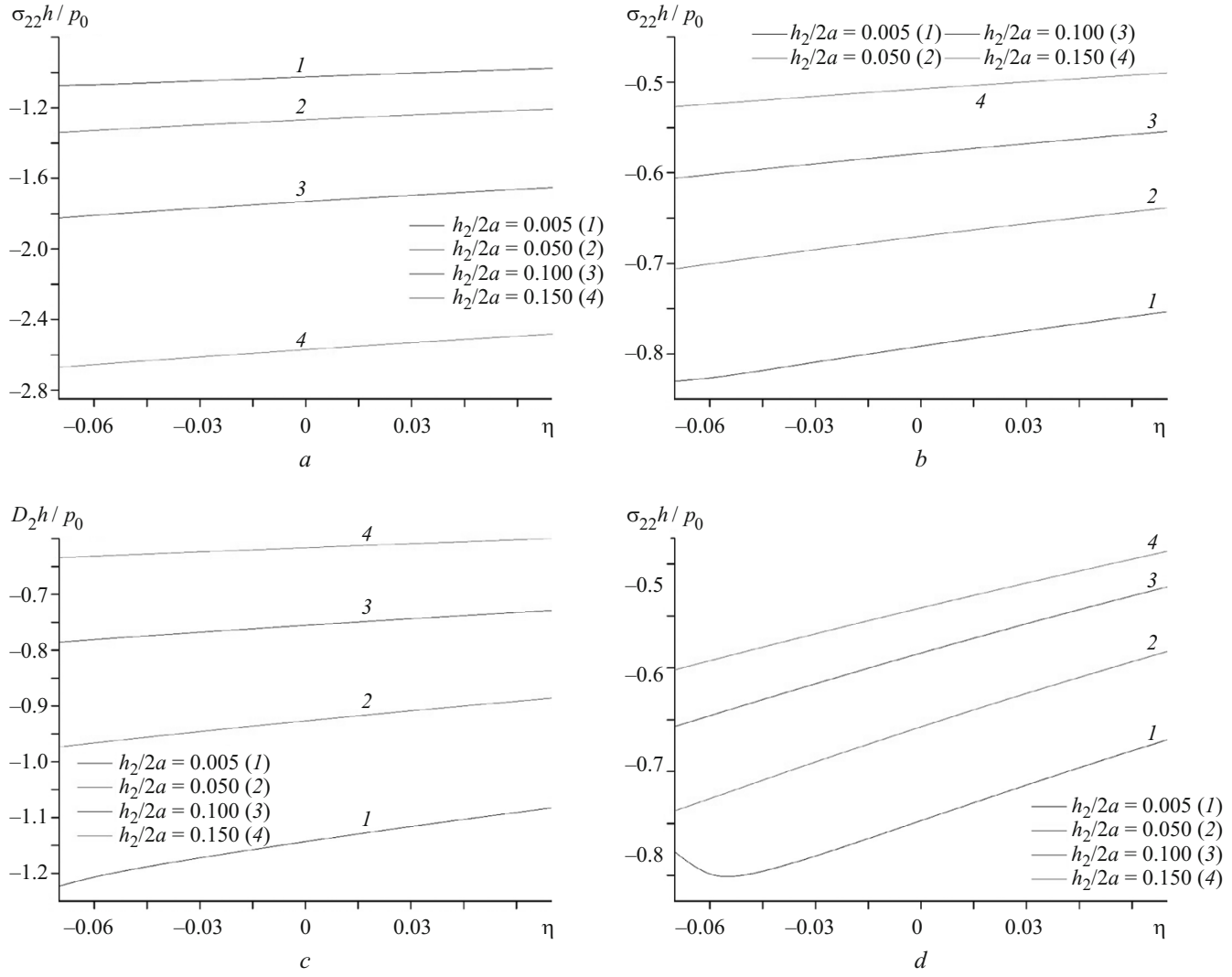

Fig. 6. Variations of $\sigma_{22}h/p_0$ and D_2h/p_0 with η for different values of $h_2/2a$ under Case I and $\Omega = 0.3$ at the points $(0,-h_1/h)$ (*a*), $(0,-h_2/h)$ (*b*, *c*), and $(0,-1)$ (*d*).

To observe the influence of a change in the thickness of the piezoelectric core on this effect, Fig. 6 displays the variations of $\sigma_{22}h/p_0$ and D_2h/p_0 with respect to the initial stress parameter η at the points $(0,-h_1/h)$, $(0,-h_2/h)$ and $(0,-1)$ under the same assumptions in Fig. 5. Both the stress $\sigma_{22}h/p_0$ and the electrical displacement D_2h/p_0 depend linearly on the initial stress parameter. It can be shown that the slope of this linear dependence increases towards to the bottom surface. The type of material used in each layer causes this result. By the same token, the slope of each graph decreases with increasing thickness of the core layer. It can be said from this result that, when the thickness of the piezoelectric core decreases, the effect of both the initial stretching and initial compression on σ_{22} and D_2 increases.

The numerical results obtained have been presented for constant values of Ω until now. But the one of the main aims of the present paper is to investigate the effect of certain problem parameters on the frequency response of the stress $\sigma_{22}h/p_0$ and the electrical displacement D_2h/p_0. Thereafter, the influence of the relevant parameters on the frequency response of $\sigma_{22}h/p_0$ and D_2h/p_0 will be analyzed at the points $(0,-h_1/h)$, $(0,-h_2/h)$ and $(0,-1)$ under Case I unless otherwise specified.

Figure 7 presents the variation of the stress $\sigma_{22}h/p_0$ and the electrical displacement D_2h/p_0 with the dimensionless frequency Ω for different values of the thickness h_2. As can be seen, the absolute values of $\sigma_{22}h/p_0$ and D_2h/p_0 decrease with the dimensionless frequency Ω. Also, while the absolute values of $\sigma_{22}h/p_0$ decrease with the thickness h_2 at $(0,-h_1/h)$, the absolute values of $\sigma_{22}h/p_0$ and D_2h/p_0 decrease with increasing thickness h_2 at the other points.

This difference in Fig. 7*a* is a natural result of its proximity to the free surface of the investigated point. It follows from the investigations of the graphs that there exist locations where $\sigma_{22}h/p_0$ and D_2h/p_0 reach the extrema for certain values of Ω.

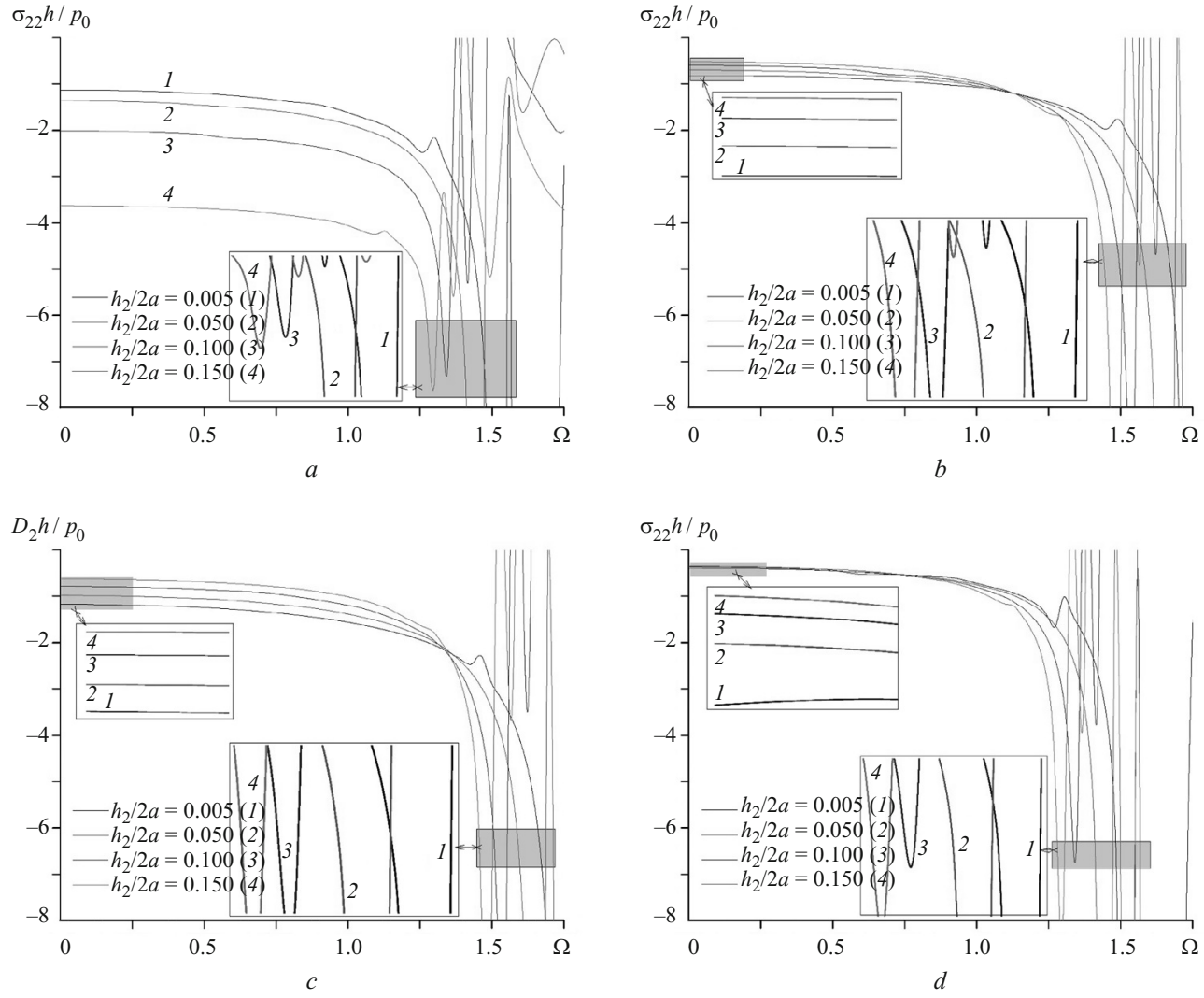

Fig. 7. Variations of $\sigma_{22}h/p_0$ and D_2h/p_0 with Ω for different values of $h_2/2a$ under Case I at the points $(0,-h_1/h)$ (*a*), $(0,-h_2/h)$ (*b*, *c*), and $(0,-1)$ (*d*).

These values are called "resonant" values and denoted by $\Omega_*^{(m)}$. The graphs show that the resonant values of Ω decrease with increasing thickness h_2. Moreover, the numerical results prove that the "resonant" values of Ω depend on the selected material and on the material type. For instance, the resonant values of Ω for the elastic layers are significantly smaller than those for the piezoelectric core. Clearly, $\Omega_*^{(\mathrm{Al})} < \Omega_*^{(\mathrm{St})} < \Omega_*^{(\mathrm{BaTiO_3})}$. An increase in the thickness h_2 causes an increase in the number of the local extremua of σ_{22} with respect to Ω. The relationships between $\sigma_{22}h/p_0$ and Ω and between D_2h/p_0 and Ω are non-monotonic. This result agrees well with the previous mechanical consideration. In addition, for $\Omega > 1.2$, the oscillating characters of $\sigma_{22}h/p_0$ and D_2h/p_0 become more sensitive for the present system. It follows from the foregoing investigations that the obtained results coincide with those in [16]. Thus, the validity and trustiness of the PC program composed by the author is confirmed again.

It can be shown from the above discussions that the oscillating character of the distribution of $\sigma_{22}h/p_0$ is similar to that for D_2h/p_0 (in qualitative sense). Thereafter, to reduce the size of the paper, all the numerical investigations are only made at the points $(0,-h_2/h)$ and $(0,-1)$ for the normal stress $\sigma_{22}h/p_0$.

The numerical results given in Fig. 8 allow us to draw certain conclusions on the influence of changes in the ratio $h/2a$ on the frequency response of the sandwich plate- strip. According to the graphs in Fig. 8, an increase in $h/2a$ causes a decrease in the number of the local maximums and minimums of $\sigma_{22}h/p_0$ with respect to the dimensionless frequency Ω. The values of

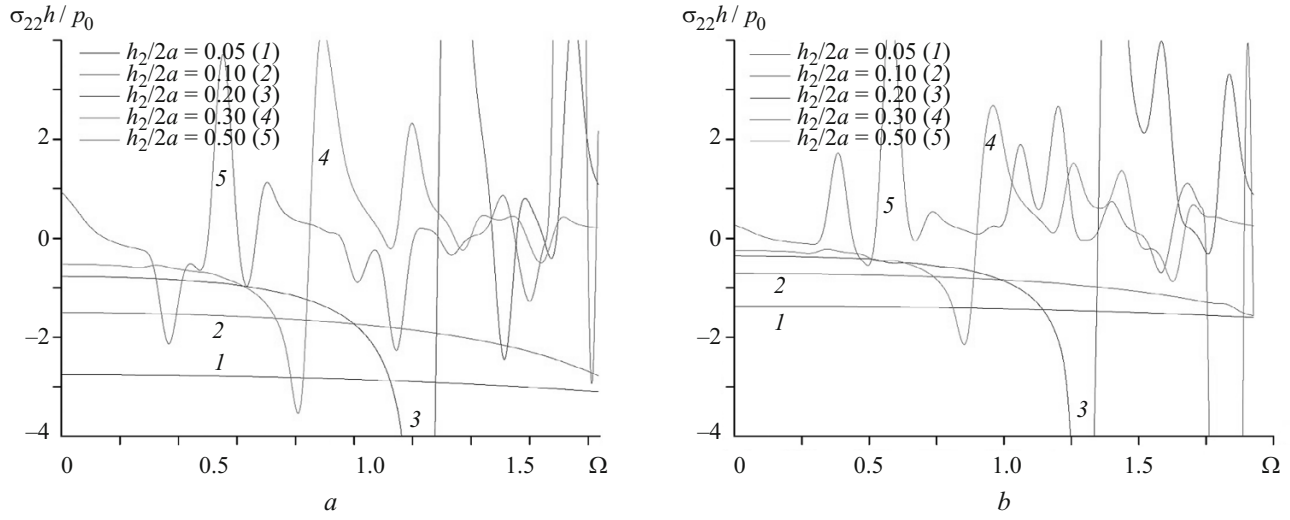

Fig. 8. Variations of $\sigma_{22}h/p_0$ with Ω for different values of $h/2a$ under Case I at the points $(0,-h_2/h)$ (*a*) and $(0,-1)$ (*b*).

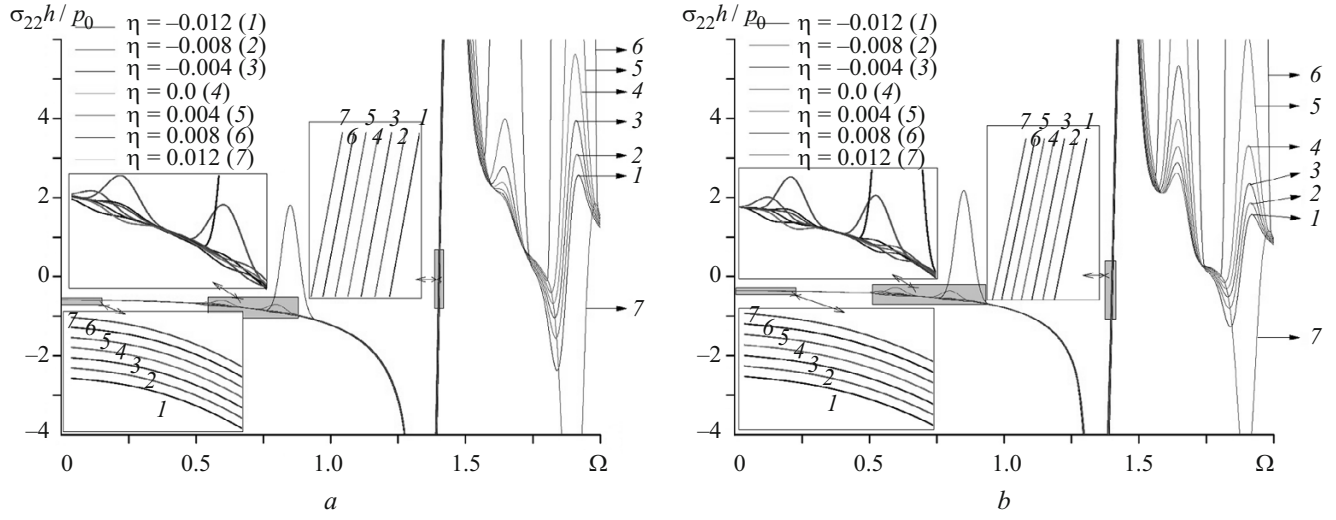

Fig. 9. Variations of $\sigma_{22}h/p_0$ with Ω for different values of η under Case I at the points $(0,-h_2/h)$ (*a*) and $(0,-h_2/h)$ (*b*).

$\Omega_*^{(m)}$ decrease with increasing ratio $h/2a$. While the values of the ratio $h/2a$ decrease, the oscillating character of the distribution of $\sigma_{22}h/p_0$ becomes more sensitive.

To investigate the effect of the initial stretching and compression parameters on the distribution of $\sigma_{22}h/p_0$ with respect to the dimensionless frequency Ω, Fig. 9 is now considered. It follows from the graphs in Fig. 9 that the influence of the initial stretching and compression parameters on the frequency response of the stress $\sigma_{22}h/p_0$ is significant not only quantitatively, but also qualitatively. Moreover, it can be shown that there exist certain locations where the parametric resonance of $\sigma_{22}h/p_0$ occurs for some values of the parameter η. An increase in the initial stretching (compression) parameter η causes an increase (decrease) in $\Omega_*^{(m)}$. If there is no initial stress, i.e., $\eta = 0$, the resonance of the current system occurs at the point where $\Omega \approx 1.2$. The initial stretching prevents the resonance value of $\sigma_{22}h/p_0$, but the initial compression exceeds the corresponding resonance value.

Figure 10 displays the effect of the parameter e on the variation of $\sigma_{22}h/p_0$ with respect to the dimensionless frequency Ω under Case II. The numerical results observed in Fig. 10 indicate that the values of $\Omega_*^{(m)}$ decrease with the parameter e. An increase in the values of the parameter e causes a decrease in the number of the local maximums and minimums

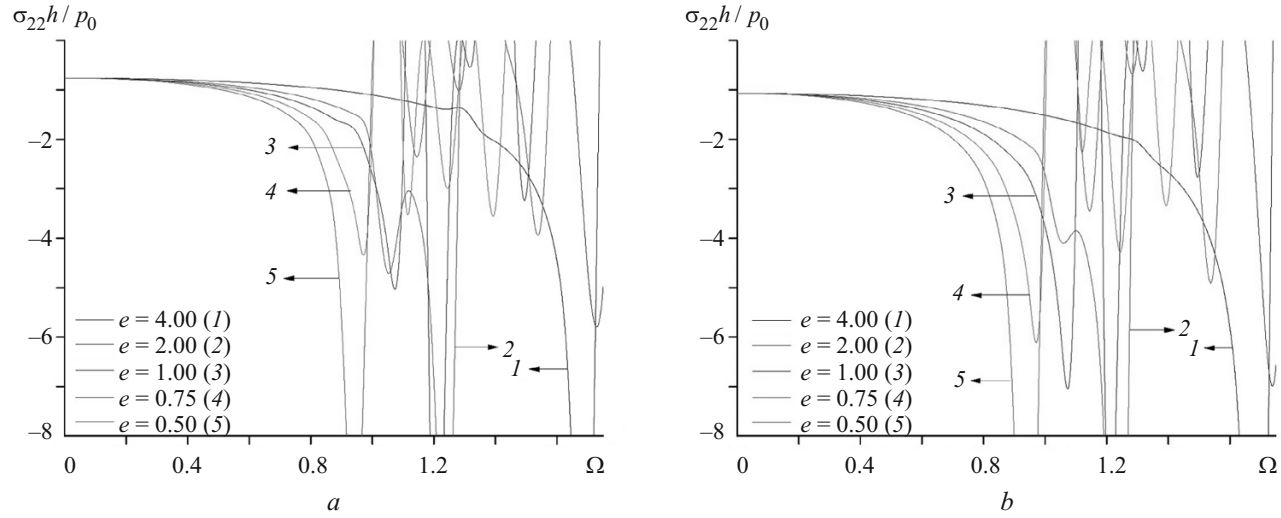

Fig. 10. Variations of $\sigma_{22}h/p_0$ with Ω for different values of e under Case I at the points $(0,-h_2/h)$ (a) and $(0,-1)$ (b).

of $\sigma_{22}h/p_0$ with respect to Ω. Moreover, when the values of Ω decrease, the effect of the parameter e on the variation of $\sigma_{22}h/p_0$ damps rapidly. The resonant values at the lower interface are less than those on the bottom surface.

5. Conclusion. In the present paper, the forced vibration problem for a pre-stressed sandwich plate-strip with a piezoelectric core perfectly bonded to two elastic layers under the action of a time-harmonic force on a rigid foundation has been investigated using the exact equations of electro-elasticity and the piecewise-homogeneous body model. The problem has been numerically solved by the finite-element method. The effect of various problem parameters on the frequency response of the sandwich plate-strip has been examined. According to all the numerical investigations, the following conclusions can be drawn:

– the effect of the initial stretching on the corresponding stress and electrical displacement components is opposite of that of the initial compression;

– an increase in the thickness of the piezoelectric core causes an increase in the number of local extrema of σ_{22} with respect to Ω;

– the resonant values of the piezoelectric material are smaller than those of the elastic materials;

– increasing the length of the plate-strip for fixed thickness or decreasing the thickness of the plate for fixed length decreases the number of the local extrema of σ_{22};

– decreasing the ratio of Young's modulus of the elastic layers decreases the resonant values of the system;

– while the initial stretching prevents the resonant value of the external force, the initial compression exceeds this resonant value.

Though the numerical results listed above have been presented under two different cases, they also have general validity in a qualitative sense. Moreover, these numerical results are encountered daily in engineering practice in impact treatment of metals that lie on one another.

REFERENCES

1. J. R. Vinson, *Plate and Panel Structures of Isotropic*, *Composite and Piezoelectric Materials*, *Including Sandwich Construction*, Springer, Dordrecht (2005).
2. A. K. Nayak, S. S. J. Moy, and R. A. Shenoi, "Free vibration analysis of composite sandwich plates based on Reddy's higher-order theory," *Composites*, *Part B*, **33**, No. 7, 505–519 (2002).
3. A. Chakrabarti and A. H. Sheikh, "Buckling of laminated sandwich plates subjected to partial edge compression," *Int. J. Mech. Sci.*, **47**, No. 3, 418–436 (2005).
4. L. Hazard and P. Bouillard, "Structural dynamics of viscoelastic sandwich plates by the partition of unity finite element method," *Comput. Meth. Appl. Mech.*, **196**, 4101–4116 (2007).

5. M. K. Pandit, B. N. Singh, and A. H. Sheikh, "Buckling of laminated sandwich plates with soft core based on an improved higher order zigzag theory," *Thin. Wall. Struct.*, **46**, No. 11, 1183–1191 (2008).
6. S. Xiang, K. Wang, Y. Ai, Y. Sha, and H. Shi, "Analysis of isotropic, sandwich and laminated plates by a meshless method and various shear deformation theories," *Compos. Struct.*, **91**, No. 1, 31–37 (2009).
7. R. Li, G. A. Kardomateas, and G. J. Simitses, "Point-wise impulse (blast) response of a composite sandwich plate including core compressibility effects," *Int. J. Solids. Struct.*, **46**, No. 10, 2216–2223 (2009).
8. T. M. Tu, L. N. Thach, and T. H. Quoc, "Finite element modeling for bending and vibration analysis of laminated and sandwich composite plates based on higher-order theory," *Comp. Mater. Sci.*, **49**, No. 4, 390–394 (2010).
9. S. M. Hasheminejad and B. Gheshlaghi, "Three-dimensional elastodynamic solution for an arbitrary thick FGM rectangular plate resting on a two parameter viscoelastic foundation," *Compos. Struct.*, **94**, No. 9, 2746–2755 (2012).
10. S. D. Akbarov and N. Yahnioglu, "Buckling delamination of a sandwich plate-strip with piezoelectric face and elastic core layers," *Appl. Math. Model.*, **37**, 8029–8038 (2013).
11. M. A. R. Loja, C. M. M. Soares, and J. I. Barbosa, "Analysis of functionally graded sandwich plate structures with piezoelectric skins using B-spline finite strip method," *Compos. Struct.*, **96**, 606–615 (2013).
12. M. Shahraeeni, R. Shakeri, and S. M. Hasheminejad, "An analytical solution for free and forced vibration of a piezoelectric laminated plate coupled with an acoustic enclosure," *Comput. Math. Appl.*, **69**, No. 11, 1329–1341 (2015).
13. A. Sankar, S. Natarajan, and M. Ganapathi, "Dynamic instability analysis of sandwich plates with CNT reinforced facesheets," *Compos. Struct.*, **146**, No. 20, 187–200 (2016).
14. A. N. Guz, *Elastic Waves in a Body with Initial* (*Residual*) *Stresses*, A.S.K., Kiev (2004).
15. J. Yang, *An Introduction to the Theory of Piezoelectricity*, Springer, New York (2005).
16. A. Daşdemir and M. Eröz, "Mathematical modeling of dynamical stress field problem for a pre-stressed bi-layered plate-strip," *Bull. Malays. Math. Sci. Soc.*, **38**, No. 2, 733–760 (2015).
17. O. C. Zienkiewicz and R. L. Taylor, *The Finite Element Method*, Vol. 1. *Basic Formulation and Linear Problems*, McGraw-Hill, London (1989).
18. Y. S. Uflyand, *Integral Transformations in the Theory of Elasticity*, USSR Academy of Science, Moscow–Leningrad (1963).